Sublingual protein delivery by a mucoadhesive patch made of natural polymers

Anne-Lise Paris, Sofia Caridade, Evelyne Colomb, Mélanie Bellina, Eléa Boucard, Bernard Verrier, Claire Monge

Acta Biomaterialia 128 (2021) 222–235

Contents lists available at ScienceDirect

Acta Biomaterialia

journal homepage: www.elsevier.com/locate/actbio

Full length article

Sublingual protein delivery by a mucoadhesive patch made of natural polymers

Anne-Lise Paris[1,*], Sofia Caridade[1,*], Evelyne Colomb, Mélanie Bellina, Eléa Boucard, Bernard Verrier, Claire Monge[*]

Laboratory of Tissue Biology and Therapeutic Engineering, UMR5305 CNRS/UCBL, 7 passage du Vercors, 69367 Lyon Cedex 07, France

ARTICLE INFO

Article history:
Received 1 December 2020
Revised 8 April 2021
Accepted 13 April 2021
Available online 18 April 2021

Keywords:
Protein delivery
Sublingual mucosa
Polysaccharide
Layer-by-layer
Freestanding membrane

ABSTRACT

The sublingual mucosa is an appealing route for drug administration. However, in the context of increased use of therapeutic proteins, development of protein delivery systems that will protect the protein bioactivity is needed. As proteins are fragile and complex molecules, current sublingual formulations of proteins are in liquid dosage. Yet, protein dilution and short residence time at the sublingual mucosa are the main barriers for the control of the dose that is delivered. In this work, a simple delivery scaffold based on the assembly of two polysaccharides, chitosan and hyaluronic acid, is presented. The natural polymers were assembled by the Layer-by-Layer methodology to produce a mucoadhesive and oro-dispersible freestanding membrane, shown to be innocuous for epithelial human cells. The functionalization of the membrane with proteins led to the production of a bioactive patch with efficient loading and release of proteins, and suitable mechanical properties for manipulation. Sublingual administration of the patch in mouse evidenced the absence of inflammation and an extended time of contact between the model protein ovalbumin and the mucosa compared to liquid formulation. The delivery of fluorescent ovalbumin in mouse sublingual mucosa demonstrated the penetration of the protein in the epithelium 10 min after the patch administration. Moreover, a migration assay with a chemokine incorporated into the patch showed no decrease in bioactivity of the loaded protein after enzymatic release. This study therefore provides a promising strategy to develop a sublingual protein delivery system.

Statement of significance

Although the oral route is largely used for drug delivery, it has limitations for the delivery of proteins that can be degraded by pH or gastric enzymes. The sublingual route therefore appears as an interesting approach for protein administration. In this work, a simple delivery scaffold is presented based on the assembly of two polysaccharides by the Layer-by-Layer methodology to produce a mucoadhesive patch. The produced patch allowed efficient loading and release of proteins, as well as protection of their bioactivity. An extended time of contact between the protein and the mucosa compared to liquid formulation was highlighted in mouse model. This study provides a promising strategy to develop a sublingual protein delivery system.

1. Introduction

Oral administration of drugs is the most widely used route of delivery. However, the *per oral* drug adsorption is limited by the presystemic drug degradation in the gastro-intestinal tract (acidic pH, degradation enzymes) and the hepatic first-pass metabolism. As a consequence, the delivery of fragile macromolecules with high molecular weight such as proteins would be compromised by this route of administration as these molecules are highly susceptible

* Corresponding authors.
E-mail addresses: Anne-lise.paris@ibcp.fr (A.-L. Paris), sofiafi26@gmail.com (S. Caridade), evelyne.colomb@ibcp.fr (E. Colomb), melanie.bellina@lyon.unicancer.fr (M. Bellina), elea.boucard@univ-nantes.fr (E. Boucard), bernard.verrier@ibcp.fr (B. Verrier), Claire.monge@ibcp.fr (C. Monge).
[1] These authors contributed equally.

https://doi.org/10.1016/j.actbio.2021.04.024

to denaturation or enzymatic degradation [1]. Considering the substantial developments in genetic engineering, biological therapeutics such as proteins are gaining large interest [2]. Thus, the exploration of alternative routes for protein delivery is a biotechnological as well as medical challenge [3]. In this context, other mucosal administration routes of therapeutic proteins, and in particular the buccal route, has been recognized as a potential alternative for the delivery of proteins such as insulin for the treatment of diabetes [4] or vaccine antigens [5]. Moreover, sublingual administration of allergens has been proven to be safe and efficient for the treatment of type I allergies but remains to be optimized by the design of platforms to improve allergen presentation to buccal dendritic cells (DCs) [6] and allow controlled protein delivery.

Indeed, oral cavity mucosa is considered as a potent administration site for protein delivery as it allows bypass of the first-pass effect, presents poor enzymatic activity, physiological range of pH and is anatomically accessible. Moreover, as a well vascularized-tissue, it offers short access to blood capillaries, and a buccal delivery system can thus provide either a local delivery (mucosal) or a systemic delivery (transmucosal) of the bioactive compound.

The oral cavity mucosa presents several sites of administration (cheeks, gingiva, lips, palate, tongue, floor of the mouth), the sublingual site being the most attractive due to its thin epithelium and high vascularization. The sublingual mucosa is covered by mucus mainly composed of water and glycoproteins called mucins, and consists in a stratified squamous epithelium composed by 6-8 epithelial layers in mouse and 8–12 cells (0.1– 0.2 mm) in human [7,8]. A basal membrane separates the epithelium from the underlying lamina propria (connective tissue) and submucosa (muscle, blood capillaries…). Once a molecule has permeated through the epithelium by transcellular (through the cells) or paracellular (in between the cells) transport, it can either enter the connective tissue containing capillaries to be delivered to the systemic circulation or being uptaken by the antigen-presenting cells (APCs) that will either induce immune regulation (tolerance) or immune response against the antigen molecule [8].

Unlike humans, a keratinized epithelium is found in oral cavity mucosa of rodents that acts as an additional protection barrier against foreign bodies. The presence of this keratinized layer (composed mainly of anucleated keratinocytes) could be considered as a bias when using mouse as an animal model for the development of a sublingual delivery system. However, all rodent and non-rodent oral cavity mucosa present limitations in permeability and overcoming these issue in rodents such as mouse would allow easy translation to human use [8]. Besides, the keratinized layer of the mouse sublingual mucosa is the thinner of all oral cavity mucosa, and already allowed interesting and promising developments in protein delivery and bioavailability along with the use of chemical penetration enhancers [9], nanoparticles or mucoadhesive delivery systems [10,11].

The actual formulations for sublingual drug delivery are found in different dosage form such as liquid, tablets, gels, chewing gum, spray or patches [12,13]. Yet, the current formulation processes rarely achieve incorporation of bioactive proteins that are sensitive to temperature, high pressure or solvents. Besides, since human salivary glands secrete around 600 mL of saliva per day [14], the dilution of bioactive compounds in saliva is a major issue in buccal delivery. Therefore, one of the main challenge in sublingual delivery is to increase the contact time between the formulation and the mucosa to ensure optimal bioavailability of the delivered molecule. Mucoadhesive systems with prolonged retention of the compound at the mucosa surface are thus required to optimize this delivery route [15,16]. For all these reasons, polymer-based systems, and in particular chitosan (CHI)-based systems were developed as sublingual protein delivery systems to improve bioavailability or targeting of their cargo [17–20]. In addition to its known mucoadhesive properties, CHI is considered as a multifunctional polymer as it also contributes to inhibit peptidase activity, presents antimicrobial activity [21] and acts as a permeation enhancer [22].

The use of a mucoadhesive system exhibiting permeation enhancement abilities would contribute in significant reduction of the dose of the administered therapeutics as well as a better control of its adsorption. In this view, we developed a mucoadhesive patch made of a combination of two polysaccharides: CHI and hyaluronic acid (HyA) which is widely present in the human saliva. The two natural polymers were assembled by the Layer-by-Layer (LbL) technology, that is a simple, inexpensive and tunable process [23]. LbL allows to build a structure by consecutive deposition of polymers with opposite charges, repeated several times by an automated process to obtain a freestanding membrane [24]. The deposition of 100 bilayers of polymers led to the production of a freestanding membrane expected to dissolve in saliva due to the presence of hyaluronidases and other enzymes able to degrade both polysaccharides. As they are polyelectrolytes with opposite charges, the electrostatic interactions between CHI and HyA can be easily tuned by pH variation thus allowing incorporation of macromolecules in its core. The protein incorporation/release abilities of the patch were assessed with a model protein, ovalbumin (OVA). As *in vitro* models often fail in predicting living tissue behavior, the investigation of mucoadhesion, inflammation and protein transport was evaluated in mouse model. Finally, the persistence of bioactivity of a model cytokine was measured by a chemotaxis assay to confirm the protective effect of our protein carrier.

2. Material and methods

2.1. Material

Medium molecular weight chitosan (CHI) was purchased from Sigma-Aldrich. Before its usage, CHI was purified by filtering steps and precipitation in water and ethanol, followed by freeze-drying having a final molecular weight of 770 kDa and a degree of deacetylation (DD) of 78%. At low pH (<6.5), CHI is a positively charged polyelectrolyte. For comparison, the polysaccharide Viscosan® (VIS) purchased from Flexichem (NAS-081, Viscosity 430 mPas, DD of 49%) was used, as it presented a distinctive distribution of the N-acetylated groups and lower DD than CHI. Sodium Hyaluronate (HyA) either with 610 kDa (HyA_{610}) or 1020 kDa (HyA_{1020}) was purchased from HTL, France and were used as received. The polystyrene substrates used for membranes production were purchased from Dutscher (Weighing cup shock-resistant #045105). All other reagents and solvents were used without purification. The hematoxylin Gill's formula, Vectastain Elite ABC kit, Vectashield with DAPI and AEC peroxidase substrate were purchased from Vector. Peroxidase blocking reagent was purchased from Dako, and the biotin rat anti-mouse I-A/I-E antibodies from BD Pharmingen. Ovalbumin alexa Fluor ™ 647 was purchased from Life Technologies, France. Anti-CCR6 rabbit polyclonal antibody alexa Fluor ™ 488 was purchased from Bioss antibodies. Protease inhibitor cocktail and BCA protein assay kit were purchased from ThermoFisher Scientific, USA. Interleukin 1 beta, IL-6 and Tumor Necrosis Factor alpha were simultaneously quantified with a V-Plex Proinflammatory Panel 1 Mouse Kit (MSD, USA) and quantified by electroluminescence using Mesoscale Discovery system (Meso QuickPlex SQ 120, MSD, USA).

2.2. Fluorescent chitosan

20 mL of medium chitosan (CHI, 770 kDa, 10 mg/mL in acetic acid 0.1 M was let to react with 20 mL of fluoresceinisothiocyanate (FITC, 1 mg/mL in dehydrated methanol) for 3 h at room temperature (RT), protected from light. pH was then raised to 10 to pre-

cipitate the CHI, followed by centrifugations at 11000 g for 15 min and several washings with H_2O until no fluorescence was detected in the supernatant. The CHI was then dissolved in 20 mL of acetic acid 0.1 M and the rest of unbound FITC was removed by dialysis (Spectrum, USA) in distilled water for 3 days in the dark, water being replaced every day. The quantity of CHI and FITC were determined by spectrophotometry at 490 nm and 270 nm respectively. Fluorescein-labeled medium weight chitosan (CHI^{FITC}) was aliquoted at 2 mg/mL in acetic acid 0.1 M and stored at −20 °C.

2.3. Fabrication of the CHI/HyA freestanding membranes

(CHI/HyA) freestanding membranes were produced using the LbL methodology using a dipping robot (DR-3, Riegler & Kirstein GmbH). Membranes were made using polystyrene substrates cleaned with sonication in ethanol and distilled water (5 min each). For all experiments, polyelectrolyte solutions were freshly prepared at 0.2% (w/v) in a sodium acetate buffer (CH_3COONa 0.2 M, CH_3COOH 0.2 M, pH = 5.5, RT). The substrates were immersed sequentially in either CHI or VIS, and HyA (either 610 kDa HyA_{610} or 1020 kDa HyA_{1020}) solutions with a washing step in sodium acetate buffer between each deposition in polymers solution. Deposition times of 3 or 6 min for polyelectrolytes and 2 or 4 min for each washing step were used and called short cycles (SC) or long cycles (LC) respectively. These immersions were repeated 100 times (total production time: 17 h for SC and 34 h for LC) and the process was finished by a CHI or VIS layer to ensure symmetric mucoadhesion of the produced membranes. The nomenclature used for these 100 bilayers was the following: $(CHI/HyA)_{100}$-CHI or $(VIS/HyA)_{100}$-VIS depending on the type of polycation used. Then the membranes were let to dry at RT. Finally, membranes were easily detached from their respective underlying substrates by peeling off with a tweezer and can be easily manipulated (Fig. 1A).

Fluorescent membranes ($(CHI^{FITC}/HyA)_{100}$-CHI^{FITC}) were prepared as described above, with 0.5% of CHI^{FITC} in the CHI solution at 2 mg/mL in sodium acetate buffer pH 5.5, protected from light.

2.4. Thickness of freestanding membranes

The thickness of the produced membranes was measured after drying and detachment from the substrate. Membrane thickness was determined using a micrometer (High-Accuracy Digimatic Micrometer, Mitutoyo). Membranes produced under the same conditions from at least 3 independent runs were analyzed and at least 5 measurements per membrane were performed.

2.5. Artificial saliva and enzymatic degradation studies

Membranes of 1 cm^2 were weighed prior to the experiment. Artificial saliva was prepared with α-amylase, hyaluronidase and lysozyme, dissolved in 0.15 M NaCl, 20 mM HEPES, pH 6.5. All enzymes had a final concentration of 100 µg/mL. Samples were soaked in artificial saliva and incubated at 37 °C under slow agitation for 30 min, 1 h, 3 h, 6 h and 24 h. After each incubation period, membranes were dried at 37 °C and weighted. The percentage of weight loss (WL) of the membranes for the different conditions was determined following Eq. (1), with Wi being the initial dry weight of the membrane and Wf being the weight of the dry membrane after each predetermined time point. Three independent experiments were conducted for each condition in triplicates and the average value was taken as the weight loss percentage.

$$WL = (Wi - Wf)/Wi \times 100 \quad (1)$$

For membrane observation by confocal laser scanning microscopy (CLSM), fluorescent membranes were immobilized on glass slides and let to incubate in artificial saliva at 37 °C under agitation during 30 min, 3 h, 6 h or 24 h. The degradation was stopped by rinsing with acetate buffer until CLSM observation with LSM710 Confocal Microscope (Carl Zeiss SAS, France). All images were analyzed using Carl Zeiss Zen Softwares and Image J Software.

2.6. Scanning electron microscopy (SEM)

The morphological analysis of the samples (after and before degradation) was performed using Scanning Electron Microscope (SEM, Merlin Compact VP, Zeiss) at an accelerated voltage of 5 kV. Both sides of the membranes were observed. Before observation, all samples were copper coated (Balzers MED 010).

2.7. Cytotoxicity assays

Immortalized Ho-1u-1 cells (human cell line from floor of mouth squamous cell carcinoma, from GIMAP, St Etienne, France) were cultured in Dulbecco's Eagle's medium (DMEM) with D-glucose (4.5 g/L), pyruvate (1 mM) and L-glutamine (2 mM), DMEM/Ham's F12 Nutrient Mixture (1:1) supplemented by 10% (v/v) heat-inactivated fetal bovine serum (FBS) and 1% (v/v) penicillin/streptomycin. HeLa cells (human epithelial cell line from adenocarcinoma, ATCC® CCL-2) were cultured in DMEM with D-Glucose (4.5 g/L), Pyruvate (1 mM) and L-Glutamine (2 mM) containing 10% (v/v) heat-inactivated FBS and 1% (v/v) Penicillin/Streptomycin. Cells were maintained at 37 °C and 5% CO_2.

Two days before cytotoxicity tests, cells were seeded in a 96-well plate. In parallel, $(CHI/HyA)_{100}$-CHI membranes were cut to size (3 cm^2 per mL of medium), sterilized by UV light and ethanol 70%, as ethanol ensures additional asepsis of cultured cells without affecting incorporation abilities of the membranes. Membranes were then let to incubate overnight at 37 °C in culture medium containing salivary enzymes (lysozyme, α-amylase and hyaluronidase) at 100 µg/mL. Culture medium was then removed from the wells and replaced by the medium containing membrane degradation products. Cells were let to incubate at 37 °C for 24 h. Then, methylthiazolyldiphenyl-tetrazolium bromide (MTT, 0.5 mg/mL) was added to each well and was let to incubate 3 h at 37 °C. A solubilization solution containing 10% (v/v) of Triton X-100 and HCl (0.1 M) in anhydrous isopropanol was then added on cells overnight at RT, protected from light. Absorbance was measured at 570 nm and 690 nm (i-control Infinite® M1000 Pro, Tecan, Switzerland). Positive controls were performed with SDS 0.1% (v/v) and negative controls with cells alone. Data were determined as the mean of three replicates and for three independent experiments.

2.8. Mice model and animal ethics

In vivo studies were conducted either on 6- to 8- week old female CB6F1 mice (Charles River Laboratories, France) at the animal facility PBES of Lyon or on male SHK-1 (Charles River Laboratories, France) for tomography in the animal facility AniCan at the Cancer Research Center of Lyon (CRCL), Lyon, France. All animals were maintained in pathogen-free conditions. All of the experiments were performed in accordance with animal welfare regulations for their use for scientific purposes governed by the European Directive 2010/63/EU. Protocols were validated by the local Animal Ethics Evaluation Committee (CECCAPP: C2EA-15) and authorized by the French Ministry of Education and Research.

2.9. Sublingual administration of membranes or solutions

Membranes were cut to fit to the size of mouse tongue (2 mm x 7 mm) and sterilized by UV light. Membranes or liq-

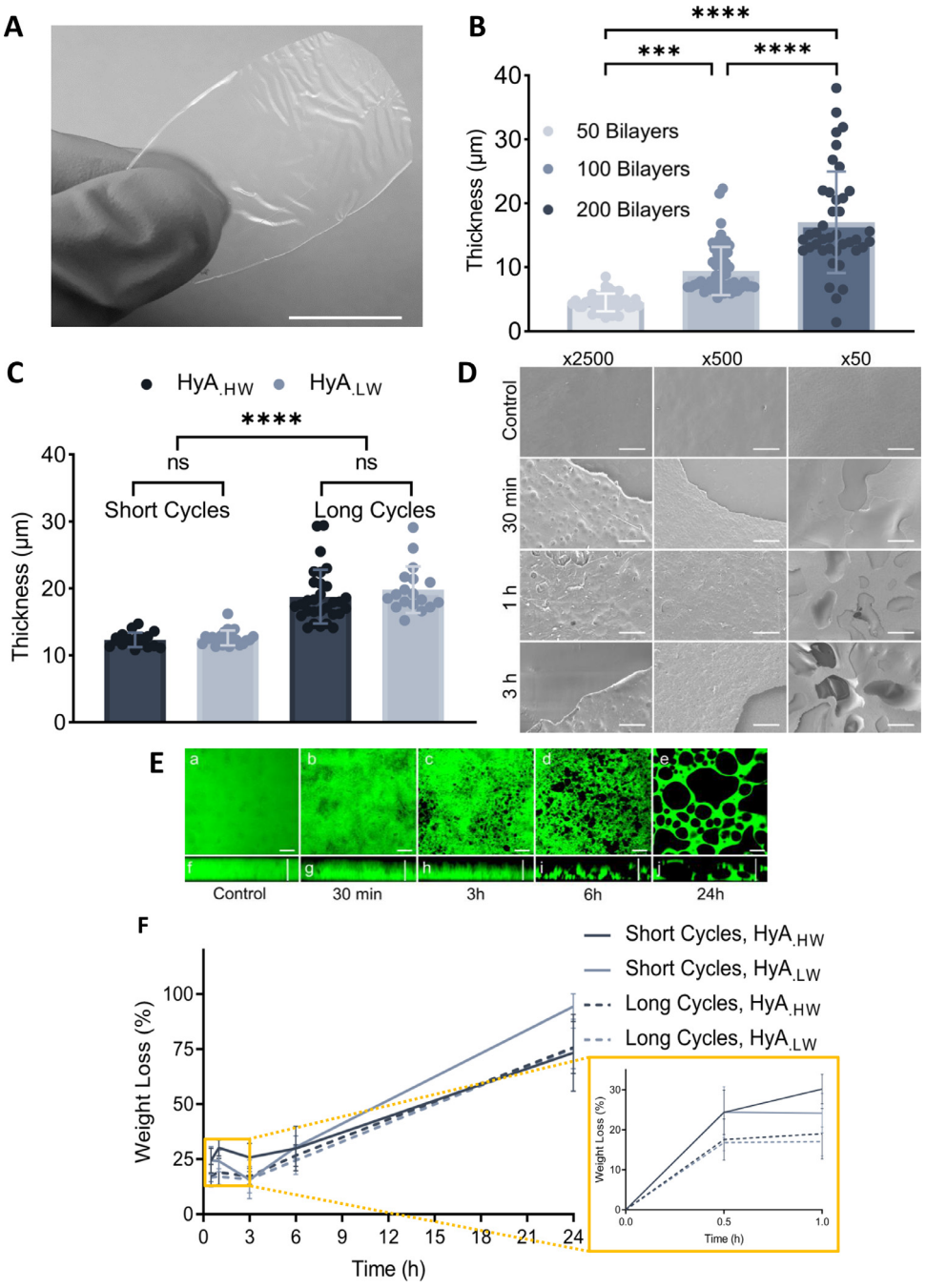

Fig. 1. Thickness and degradation profiles of freestanding (CHI/HyA)100 membranes. (**A**) Photography of a $(CHI/HyA_{660})_{100}$ membrane after Layer-by-Layer production by using short cycle deposition. Scale bar: 2 cm (**B**) Membranes thickness by varying the number of bilayers (50, 100 or 200 bilayers). (**C**) Thickness of the membranes by varying the HyA molecular weight (660 or 1020 kDa) or the deposition time: short cycles or long cycles. (**D**) SEM pictures of (CHI/HyA_{660})-CHI short cycles immersed in artificial saliva during 30 min, 1 h or 3 h. Scale bars represent 9 µm, 45 µm and 450 µm for x2500, x500 and x50 magnification, respectively. (**E**) Pictures of (CHI^{FITC}/HyA_{660})-CHI^{FITC} short cycles by confocal microscopy after 30 min, 3 h, 6 h or 24 h in artificial saliva. The control corresponds to the immersion of the membrane in acetate buffer for 24 h. a, b, c, d, e: surface of the membrane; f, g, h, i, j: z-section images of the top picture. Horizontal scale bar: 50 µm, vertical scale bar: 30 µm. (**F**) *In vitro* degradation profile of membranes immersed in artificial saliva quantified as the percentage of weight loss as a function of the parameters for the membranes production. Statistical significance of differences was determined using nonparametric Kruskal-Wallis with Dunn's post hoc test; ns: non-significant; ***p < 0.001, **** p < 0.0001. Error bars are ± SD.

uid formulations were then administered sublingually (ventral part of the tongue) to slightly anesthetized mice (isoflurane 4%). After administration, a gentle pressure was exerted during 10 s (until wake up) on the dorsal part of the tongue to ensure contact of the membrane or the liquid solution with the mucosa. No further contention was performed. Once the animal recovered from anesthesia, they were let free to swallow or groom. Water and food was removed for the next 30 min after administration.

2.10. Histological analysis of mucosal swelling and MHC-II cell recruitment

Native membranes, HCl-treated membranes (incubation 1 h in 1 mM HCl, pH 3) and NaCl-treated membranes (incubation 1 h in NaCl 0.15 M, HEPES 0.02 M, pH 6.5) membranes were administered. A drop of 12.5 µl of 0.5% 1-fluoro-2.4-dinitrobenzene (DNFB) solution applied under the tongue of mice was used as positive

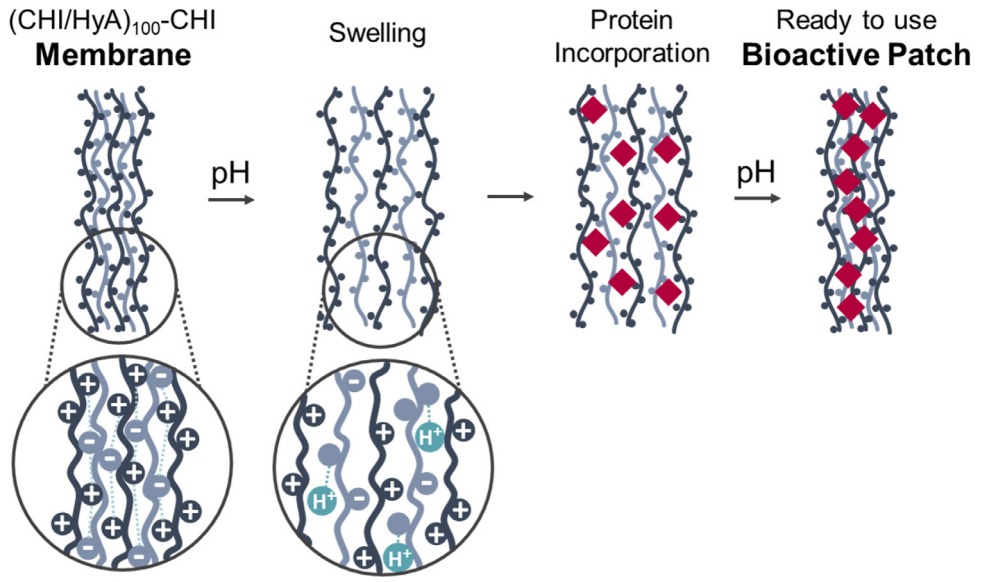

Scheme 1. Schematic representation of protein incorporation in LbL assembly by pH variation. After functionalization by protein entrapment through the variation of pH and structural changes on the assembly, the LbL membrane becomes a bioactive patch, ready to be administered.

control of inflammation. The negative control group were not subjected to any manipulation. Each group was composed of 2 to 5 mice. Right after administration of the sublingual formulations, the mice were alert and water was removed for the first 30 min. At each time point (30 min, 60 min, 2 h or 6 h according to the groups), the mice were euthanized by cervical dislocation. Then, tongues were carefully cut and embedded in OCT compound and stored at −80 °C until cryosection. For the cryosection, 6 µm thick sections were performed using a Cryostat (LEICA) and fixed on glass slides with acetone at −20 °C.

For MHC-II staining, the tongue sections were first incubated with peroxidase blocking reagent, then with biotin rat anti-mouse I-A/I-E antibodies, revealed using the Vectastain Elite ABC kit and the AEC peroxidase substrate, and finally counterstained with hematoxylin Gill's formula. The images of tongue sections were captured using an inverted microscope (Nikon Ti-E microscope). Analysis of mucosal swelling and MHC-II positive cell counting were done on 2 mm ventral surface lengths starting from the base. Epithelium and lamina propria were manually outlined on 2 mm length using the polygon tool from the image J software. Then for each region of interest, surface measurements were carried out and MHC-II positive cells were manually counted.

2.11. Samples preparation for cytokines quantification

Each group was composed of 3 mice. Two groups received native membranes or HCl-treated membranes. Three other groups of mice received sublingually 10 µL of either CHI (770 kDa, 2 mg/mL in sodium acetate buffer pH 5.5), HyA (610 kDa, 2 mg/mL, in sodium acetate buffer pH 5.5) or the combination of both polymers. Control groups of mice received sublingually 10 µL of PBS for negative controls and 12.5 µL DNFB, 0.5% (v/v) in chloroform as positive control.

Tongues were excised 6 h after membranes or solutions administration, flash freezed in liquid nitrogen and kept at −80 °C. Tissues were prepared as previously described [25]. Briefly, tongues were let to incubate on ice 2 h in RIPA buffer (Tris HCl (50 mM), NaCl (150 mM), Triton X-100 (1%), 0.5% Sodium Deoxycholate, SDS (0.1%) EDTA (1 mM) and a protease inhibitor cocktail (1%) after homogenization using scissors. They were then disrupted using a bead beater (2 × 5 min, 30 Hz, 4 °C) (TissueLyser II, Qiagen, Germany) and by sonication (2 min, 60 Hz), followed by centrifugation at 10000 rpm for 10 min at 4 °C. Total protein concentration in supernatants was then determined using BCA protein assay kit. Interleukin 1 beta (IL-1β), IL-6 and Tumor Necrosis Factor alpha (TNF-α) were simultaneously quantified in each sample by electroluminescence. Data were determined as the mean of two replicates and three mice per condition.

2.12. Protein incorporation by pH swelling

In order to assess the ability of membranes to incorporate protein in their core at different pH, membranes were equilibrated with either 1mM HCl (pH 3-3.5) or NaCl buffer (NaCl 0.15 M, HEPES 0.02 M, pH 6.5) or phosphate-buffered saline (PBS 1X, pH 7.4) at RT during 1 h. Prior to the experiments, membranes of 12 mm diameter were sterilized by UV light for 20 min. After equilibration, the excess of HCl or NaCl was removed and a drop of protein (100 µL) was added on the top of the membrane. The protein used was either ovalbumin labeled with Alexa Fluor 647 (OVA^{AF647}) at 5 µg/mL (500 ng loaded) or the cytokine CCL20 at 0.25 µg/mL (25 ng loaded) in 1mM HCl or NaCl buffer. The membranes were left to incubate at 4 °C overnight. The functionalized membranes were then named bioactive patch (Scheme 1). Except whenever clearly stated, HCl was used for protein incorporation in subsequent experiments.

2.13. Ovalbumin release study

OVA^{AF647} was incorporated according to the pH swelling method described above. The release of the protein was followed at different pH using acetate buffer (pH 5.5), PBS (1X, pH 7.4) or artificial saliva (pH 6.5) as release media. After incorporation and drying, 250 µL of release media was added on the 12 mm disks and immediately collected and saved to assess the amount of unbound protein. The release of OVA^{AF647} from the membrane was performed for 2 h with collection times at 10, 20, 30, 40, 60, 90 and 120 min. An additional sample at the time point 24 h of release in artificial saliva (after HCl incorporation) was also collected. The analysis of the released OVA^{AF647} was performed by fluorescence spectroscopy (Infinite M1000, Tecan) with the excitation/emission wavelength of Alexa Fluor 647 set at 650/668 nm. A

calibration curve for the labeled protein in PBS, acetate buffer, HCl and artificial saliva was performed at the previously mentioned wavelengths.

2.14. Dynamic mechanical analysis (DMA)

The mechanical/viscoelastic properties of the native membranes, HCl-treated membranes and the OVA-loaded bioactive patches were evaluated using Dynamical Mechanical Analysis (DMA). The DMA experiments were performed using an Artemis 242E (Netzsch, Selb, Gerrmany), equipped with the tensile mode. The samples were cut with approximately 4 mm width. The geometry of the samples was measured accurately for each sample, where the thickness was determined in three different regions using a micrometer (High-Accuracy Digimatic Micrometer, Mitutoyo). The measurements were carried out at 25 °C in the dry state, as it is intended to apply a dry patch *in vivo*. The samples were clamped in the DMA apparatus with a gauge length of 6 mm. The DMA spectra were obtained during a multi-frequency scan of 1, 2, 5 and 10 Hz. The experiments were performed under constant strain amplitude (10 µm). At least three specimens were tested for each condition with the same experimental settings.

2.15. Tomography analysis of patch mucoadhesion and protein residence time

For tomography analysis of protein residence time in the sublingual region of mice, groups of 2 mice were anesthetised in an isoflurane chamber at 4% flow for 5 min. For solution administration, 10 µL of OVA^{AF647} solution was deposited at the base of the ventral side of mice tongues. For patch administration, patches were placed on the ventral surface of the tongues. For each formulation, 5 µg of OVA^{AF647} was administered. The mice were placed in the tomography chamber (FMT 4000, Perkin Elmer), under isoflurane, in supine position for image acquisition 2, 10 or 30 min after administration.

2.16. Mucosal penetration by confocal microscopy

OVA^{AF647} penetration in the sublingual mucosa was assessed by administration of liquid formulation (10 µL) or patch $(CHI^{FITC}/HyA)_{100}$. OVA^{AF647} was incorporated into the patch by HCl treatment, as described above. Groups of 2 mice received the different formulations and were euthanized by cervical dislocation 2, 10 or 30 min after administration. Sublingual mucosa (tongue and floor of the mouth) were collected, embedded in OCT and stored at −80 °C. Cryosections of 40 µm were performed, stained with the nuclear stain DAPI and observed with a confocal microscope (LSM 710, Zeiss, Germany) with a 40x objective.

2.17. Chemotactic assay

Mouse dendritic cell line (DC 2.4, #SCC142 Milipore) was used to test *in vitro* chemotactic effect of the CCL20 chemokine delivered from the developed membranes. DCs were cultivated in RPMI medium Glutamax suplemented with 10% foetal bovine serum, 10mM HEPES, 50µM β-mercaptoethanol and 1x non-essential amino acids (later referred as growth medium, GM) at 37 °C and 5% CO_2.

Prior to chemotactic assay, a staining of the CCL20 receptor, identified as the chemokine receptor-6 (CCR6), was performed. For CCR6 staining, DCs were cultured in GM containing CCL20 with a density of 2×10^5 cells on Labtek chamber slides (12 well chamber, Ibidi®) for 24 h. The cells were then fixed with acetone, incubated with anti-CCR6 rabbit polyclonal antibody conjugated to alexa-fluor 488 and finally mounted using Vectashield wih DAPI. Images were captured using an inverted microscope (Nikon Ti-E microscope).

The chemotactic assay was carried out in ThinCert™ Cell Culture Inserts 12 Well (Greiner Bio-One 665 610) for 20 min. Prior to the assay, membranes, CCL20 and CCL20-loaded membranes (50 ng) were incubated for 24 h in salivary enzymes (100 µg/mL of α-amylase, hyaluronidase and lysozyme dissolved in GM without FBS) at 37 °C under slow agitation. Then, inserts of the 12-transwell plate were seeded with a density of 2×10^5 cells/insert and incubated for 10 min at 37 °C. Afterwards, the lower chambers of the 12-well plate were carefully filled with 1mL of chemotactic or control solutions for 10 min at 37 °C. Negative control corresponded to DCs incubated only with GM. Finally, inner sides of each inserts were wiped using cotton swabs. After fixation (paraformaldehyde 4%) and staining with DAPI, 5 pictures of each conditions were taken with an inverted microscope (Nikon Ti-E microscope). Nuclei were analyzed by 'particle analysis' using Image J software. Results are given as the average of triplicates of 3 independent experiments.

2.18. Statistical analysis

All data were analyzed and plotted in GraphPad Prism version 7.0. Experimental values are expressed as means ± standard deviation (SD) of at least three replicates; except for release data represented as mean ± standard error of the mean (SEM). Shapiro-Wilk normality test was used to verify if values were normally distributed. If normal distribution, one-way ANOVA with Tukey's multiple comparisons test was used. Otherwise, nonparametric Kruskal-Wallis with Dunn's multiple comparisons test was used, or Mann Whithney test for only two independent conditions. A value of $p < 0.05$ was considered statistically significant.

3. Results

3.1. Characterization and degradation of freestanding membranes in artificial saliva

Native (CHI/HyA) membranes were produced by varying 4 parameters: number of bilayers, HyA molecular weight (610 or 1020 kDa), the deposition time in both polyelectrolytes and rinsing solutions, and polycation (CHI *vs* VIS) properties. The influence of such parameters was firstly investigated over the membrane thickness. The growth of native (CHI/HyA) membranes was shown to be linear with 50 bilayers (4,5 ± 1,39 µm), 100 bilayers (10,30 ± 7.67 µm) and 200 bilayers (17,04 ± 7,96 µm) (Fig. 1B). At least 50 bilayers were required for easy manipulation without any post proceeding treatments, but 100 bilayers were used for the rest of the study to ensure robustness of the membranes and thickness homogeneity for protein incorporation. The use of VIS, which possesses a different viscosity and degree of deacetylation (DD), did not affect the average thickness of the membranes, but exhibit higher thickness heterogeneity as expressed by error bars representing the standard deviation (Figure S1A). Likewise, no significant differences were found on the membrane thickness by varying the molecular weight of HyA (610 kDa or 1020 kDa) (Fig. 1C). Concerning the deposition time, i.e. long cycles (6 min for the polyelectrolytes and 4 min for the rinsing buffer) and short cycles (3 min for the polyelectrolytes and 2 min for the rinsing buffer), significant differences were found over the membrane thickness where an increase of around 30% was quantified when the membranes were produced under long cycles, independently of HyA molecular weight (Fig. 1C).

The influence of the conditions that were employed for the membranes build-up was also explored in terms of degradation. Moreover, as the intent is to use the membranes for sublingual

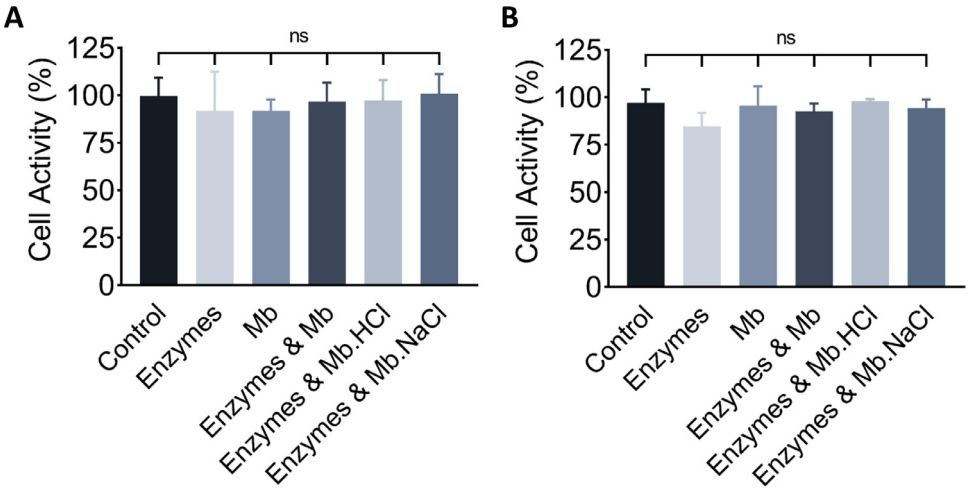

Fig. 2. Membranes degradation products show no toxicity on human epithelial cells. Cell activity after incubation of (**A**) HeLa and (**B**) Ho-1u-1 cells with degradation products during 24 h. Mb: $(CHI/HyA)_{100}$ membranes; Mb.HCl: HCl-treated $(CHI/HyA)_{100}$ membranes; Mb.NaCl: NaCl-treated $(CHI/HyA)_{100}$ membranes. Each value provided is the average of triplicates of three independent experiments (N = 3). Statistical significance compared to the control group was determined using one-way ANOVA with Tukey's post hoc test; ns: non-significant. Error bars are ± SD.

applications, an artificial saliva was produced. The artificial saliva was composed of a physiological solution containing α-amylase, lysozyme and hyaluronidase, three enzymes found in human saliva [26,27].

In order to have morphological information about their degradation, $(CHI/HyA)_{100}$ membranes were observed by SEM and confocal microscopy. By observing the images from the two techniques, an initial surface erosion was observed at 30 min, followed by the formation of superficial holes at 1 h and finally deeper holes at 3 h (Fig. 1D and Fig. 1E). The enzymatic degradation of the surface of the membrane was also observed in hydrated conditions where the membrane swelled to around 30 µm (Fig. 1E). No degradation was observed after 24 h in acetate buffer (Fig. 1E, control).

The degradation of membranes was followed over a period of 24 h and quantified as the percentage of weight loss. The membranes built with VIS were degraded faster than CHI-based membranes (Figure S1B), as expected by the fast biodegradability of VIS. Although the general profile of degradation of CHI-based membranes was not drastically affected by the molecular weight of HyA, nor the deposition times (Fig. 1F), in the early phase of the degradation process (from 0 to 1 h) a delay was observed with the membranes built under long cycles (inset in Fig. 1F). At the end of 24 h all the membranes reached a weight loss from 75% to 95%.

As these membranes were designed for mucosal administration, we selected membranes made of CHI instead of VIS to ensure prolonged delivery of the cargo protein at the early stages of degradation in contact to the mucosa. Membranes that were produced under short cycles were also selected to decrease the time of production, and the 610 kDa HyA was randomly selected as no difference in thickness nor degradation was observed as compared to 1020 kDa HyA. To ensure optimal mucoadhesion, all membranes used for animal experiments had CHI as first and last layer. Thus, for subsequent studies, $(CHI/HyA_{660})_{100}$-CHI membranes were just referred as $(CHI/HyA)_{100}$.

3.2. Cytotoxicity on human epithelial cells

The cytotoxicity of the degradation products of the membranes was tested on two human epithelial cell lines (HeLa and Ho-1u-1) over an incubation period of 24 h. No toxicity was observed on the two cell lines as the viability remained around 100% (Fig. 2A and B). This result is explained by the known biocompatibility of the two polysaccharides used to produce the membranes that were not chemically modified. The combination of the polymers did not affect their biological innocuousness. Therefore, the membranes could be applied *in vivo* on the sublingual mucosa, without any cytotoxic effect for the epithelial cells of the tissue.

3.3. Inflammatory pattern of mouse sublingual mucosa

The *in vivo* inflammatory pattern of the patch was assessed on mice through the evaluation of different hallmarks of the inflammatory status. As a positive control for inflammation, 0.5% of the hapten 1-fluoro-2.4-dinitrobenzene (DNFB) was used as it was shown to induce a transient local inflammatory (enlarged blood vessels and oedema of the lamina propria with immune cell infiltrates) when administered on the oral cavity mucosa [28]. First, the swelling surface of epithelium and lamina propria of mouse sublingual mucosa in different conditions was investigated by histology. A swelling of more than 30% of the mucosa was observed 30 min after DNFB administration compared to the control mouse that is mainly due to the swelling of the lamina propria (Fig. 3A). Noteworthy, this swelling is resorbed 2 h after DNFB administration (Figure S2A). In order to quantify the swelling induced by the $(CHI/HyA)_{100}$ membrane, native as well as HCl-treated and NaCl-treated membranes (both treatments used for protein incorporation) were applied to the sublingual mucosa during 30 min. No significant swelling was observed 30 min (Fig. 3A) nor 60 min (Figure S2A) after patch administration.

In order to correlate tissue swelling with immune cell infiltration, an immunohistochemistry staining of major histocompatibility complex class II (MHC-II) was performed. MHC-II is a major marker of APCs, in particular Langerhans cells (LCs), DCs, B lymphocytes and macrophages. The MHC-II$^+$ cell infiltrate in the mucosa was significantly decreased (around 35%) 30 min after DNFB administration (Fig. 3B and 3C). However, the native or treated membranes did not cause MHC-II$^+$ cell infiltration 30 min or 60 min after their administration and show similar pattern as the control (Fig. 3B and S2B).

To identify the global inflammation profile induced by the sublingual formulations, the expression profiles of inflammatory cytokines were quantified 6 h after administration of polysaccharides in solution, native, HCl- or NaCl-treated membranes. In all the conditions tested, the levels of IL-1β, IL-6 and TNF-α were similar to the control levels (PBS administration) (Fig. 3D, 3E and 3F).

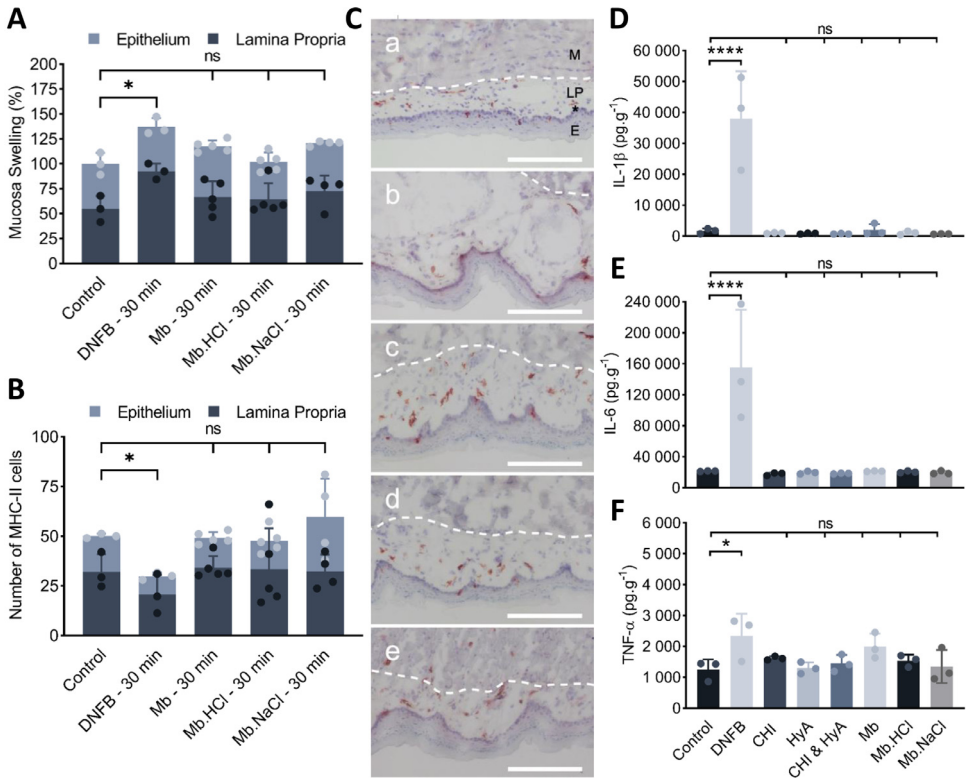

Fig. 3. Evaluation of the inflammation of the sublingual mucosa after sublingual administration of HCl- and NaCl-treated membranes. The mucosa swelling (**A**) and MHC-II$^+$ cell recruitment (**B**) were evaluated in the whole mucosa (epithelium and lamina propria) after DNFB (1-fluoro-2,4-dinitrobenzene) or membrane application. Native membranes (Mb) were administered for 30 min and HCl- treated (Mb.HCl) or NaCl-treated (Mb.NaCl) membranes were applied for 30 min. Each value provided is the average of at least 3 measurements and three independent individuals. (**C**) Representative pictures of MCH-II$^+$ cell recruitment in the mucosa by histological staining. (a) control, (b) DNFB, (c) Mb, (d) Mb.HCl, (e) Mb.NaCl. M: muscle, LP: lamina propria, E: epithelium, *: basal lamina. Scale bar: 170 µm. (**D**/**E**/**F**) Levels of inflammatory cytokines in tongue and sublingual tissues 6 h after membranes administration to mice: IL-1β (**D**), IL-6 (**E**) and TNF-α (**F**). CHI: chitosan, HyA: hyaluronic acid. Statistical significance compared to the control group was determined using one-way ANOVA with Tukey's post hoc test; ns: non-significant, *p $<$ 0.05, **** p $<$ 0.0001. Error bars are ± SD.

3.4. Incorporation/release of a model protein, ovalbumin

To evaluate the $(CHI/HyA)_{100}$ membranes as protein delivery systems, they were functionalized with a model protein, ovalbumin labeled with the fluorescent dye AlexaFluor 647 (OVA^{AF647}). OVA^{AF647} was incorporated in the membranes after equilibration of the membranes in HCl 1 mM, pH 3. To evaluate protein incorporation, a first "rinsing" was performed with various release media (*i.e.* acetate buffer pH 5.5 (rinsing buffer used for membrane build-up), PBS pH 7.4 or artificial saliva pH 6.5) by deposing a drop of solution and immediately removing it to assess the amount of unbound protein. This rinsing of the membranes with acetate buffer allowed the incorporation of 98% of OVA^{AF647} whereas rinsing with PBS led to a slight decrease in the incorporation rate (94%) (Table 1). The release kinetics over 2 h confirmed these discrepancies as, in acetate buffer less than 7% of OVA^{AF647} was released from the patch compared to 31% in PBS (Fig. 4A). When immersed in artificial saliva, 35% of OVA^{AF647} was released from the patch over 2 h (Fig. 4A), and around 90% after 24 h of immersion (Table 1).

The profile of OVA^{AF647} incorporation at pH 3 followed by rinsing by acetate buffer as release media showed that around 80% of the protein was incorporated within the first 10 µm below the surface, corresponding to one third of the full hydrated thickness (Fig. 4B and 4C). The functionalized membranes became thus an asymmetric patch with the surface presenting the protein being the one in contact with the mucosa.

As some proteins may be sensitive to acidic pH (denaturation, loss of activity…), incorporation of OVA^{AF647} was also performed at physiological pH 7.4 in PBS instead of HCl pH 3. However, it was not possible to visualize the patch by confocal microscopy after protein incorporation due to the significant swelling of the membrane. Furthermore, the instability of the structure led to an incorporation rate lower than 60% (Table 1). Instead, NaCl buffer (NaCl 0.15 M, HEPES 0.02 M, pH 6.5) was used for protein incorporation. For membrane rinsing, the same solutions were tested (acetate buffer, PBS and artificial saliva). As observed for the loading at acidic pH, rinsing with acetate buffer led to 94% of protein incorporation whereas rinsing with PBS led to only 85% of OVA^{AF647} incorporation (Table 1). The release profiles confirmed that acetate buffer ensures protein retention inside the membrane as less than

Table 1
Summary table of incorporation rates of OVA^{AF647} in $(CHI/HyA)_{100}$ membranes. The incorporation rates correspond to the initial adsorbed amount (%) of OVA on the $(CHI/HyA)_{100}$ membranes and are provided for the 3 solutions used for protein incorporation at different pH (HCl pH 3, PBS pH 7.4 and NaCl pH 6.5) and for 3 release media (acetate buffer pH5.5, PBS pH7.4 and artificial saliva pH6.5). The final adsorbed amount (%) of OVA incorporated on the $(CHI/HyA)_{100}$ membranes after 24 h of release by using artificial saliva as release media is also presented. The $(CHI/HyA)_{100}$ membranes were loaded with an initial concentration of OVA of 5 µg/mL.

Incorporation Buffer	Release media	Incorporation (%)
HCl	Acetate buffer	98 ± 5.0
HCl	PBS	94 ± 7.0
HCl	Artificial saliva	99 ± 1.0
HCl	Artificial saliva (24h)	10 ± 4.0
PBS	Acetate buffer	56 ± 15
NaCl	Acetate buffer	94 ± 6.0
NaCl	PBS	85 ± 8.0
NaCl	Artificial saliva	70 ± 7.0

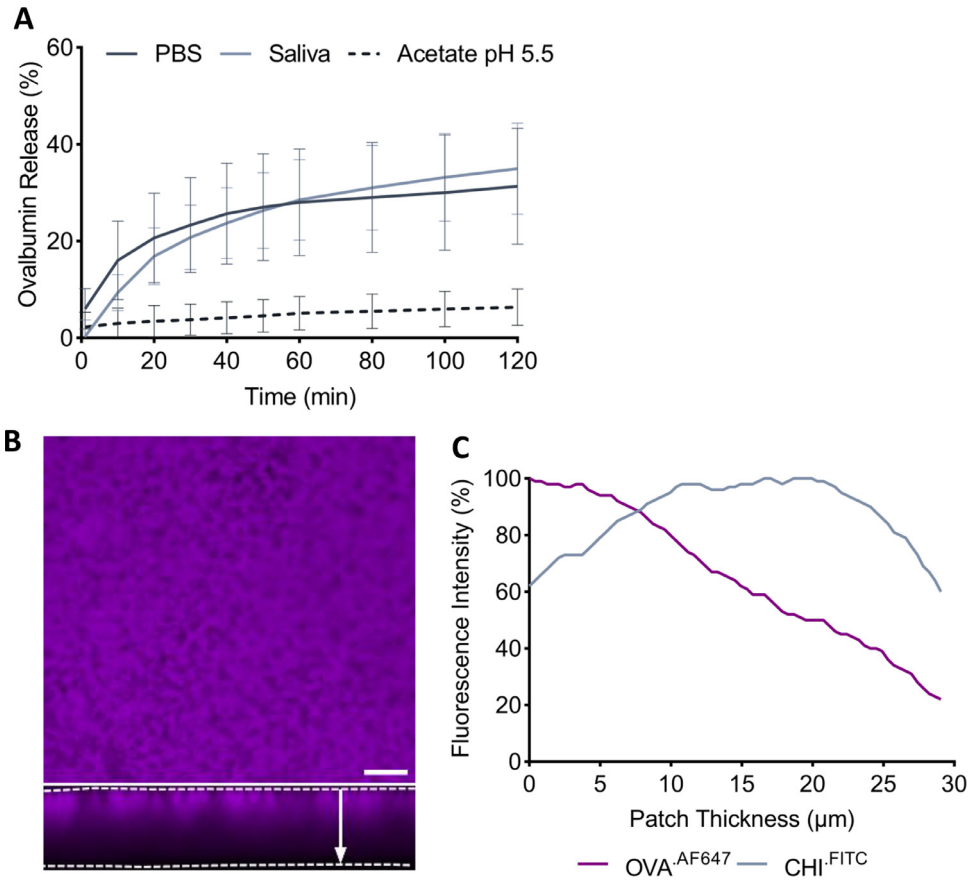

Fig. 4. Incorporation in HCl and release profiles of OVA^{AF647} from the membrane. (A) Profiles of OVA^{AF647} incorporated in HCl and released from the patch during 2 h of rinsing with different solutions. Data are the mean of triplicates and three independent experiments (N = 3). Error bars are ± SEM. (B, top) Confocal image of the surface of the patch containing OVA^{AF647}, scale bar: 50 µm. (B, bottom) Optical section of the patch along Z axis. The dotted lines represent the borders of the patch. (C) Fluorescence intensity of OVA^{AF647} and the patch (CHI^{FITC}) along the arrow represented in (B, bottom).

approximately 10% of OVA^{AF647} was released from the membrane over 2 h, whereas PBS led to a release of 36% and the release in artificial saliva reached 69% (Figure S3A). Moreover, the protein distribution within the patch was found to be more homogeneous than HCl incorporation and did not present any gradient of penetration along Z axis (Figure S3B and S3C). In all subsequent experiments, HCl was used for protein incorporation since it ensured an asymmetric incorporation with a maximum quantity of protein on one side. This specificity allows a unilateral release on the side adhered to the mucosa and limits release in the saliva on the other side, without needing to use a less degradable protective layer on this side.

3.5. Dynamic mechanical analysis

DMA experiments were performed to evaluate the effects of the incorporation of OVA on the mechanical/viscoelastic properties of the membranes. These experiments were conducted with the samples in the dry state to mimic the conditions of the final application as a dry patch on the sublingual mucosa. The storage (elastic) modulus *E'* and the loss factor (tan δ) were determined (Fig. 5). Overall, for all the samples studied, *E'* increased slightly with frequency as previously shown on similar assemblies [24]. No significant differences were found between native and the HCl-treated membranes. However, the bioactive patches, i.e. for the membranes containing OVA, an increase of stiffness by a factor 2 was observed, from around 2 GPa to 4 GPa (Fig. 5A).

Tan δ provided information about the damping properties of the membranes. It was determined that tan δ remain stable for all 3 samples at all frequencies (Fig. 5B). However, the native and the HCl-treated membranes presented slightly higher dissipative properties than the OVA-loaded patch, which can be related to their lower stiffness.

3.6. Mucoadhesion and residence time of the protein cargo

The mucoadhesion of the patches was assessed *in vivo* by visualization of the membrane lying on the sublingual mucosa 20 min after administration (Fig. 6A). The tracking of OVA^{AF647} by fluorescence molecular tomography highlighted the rapidity of dispersion of the protein after administration as liquid formulation (Fig. 6B). During the first minutes of image acquisition, OVA^{AF647} was already distributed along the digestive tract and no signal was detectable in the mouth after 10 min. When co-administered with the patch, OVA^{AF647} was detected as a concentrated signal in the mouth during at least 30 min.

3.7. Mucosal presentation and penetration of the cargo protein

The mucosal penetration of OVA^{AF647} was tracked by confocal microscopy. Even though the signal intensity 2 min after administration of OVA^{AF647}in liquid form was visible at the mucosal surface at high magnification (40x objective, zoom 2, data not shown), no signal was detectable in the selected conditions of image acquisition (40x objective) (Fig. 7). Therefore, no control of liquid OVA^{AF647} application was performed at the longer time points. On the contrary, a clear staining of OVA^{AF647} was observed at the

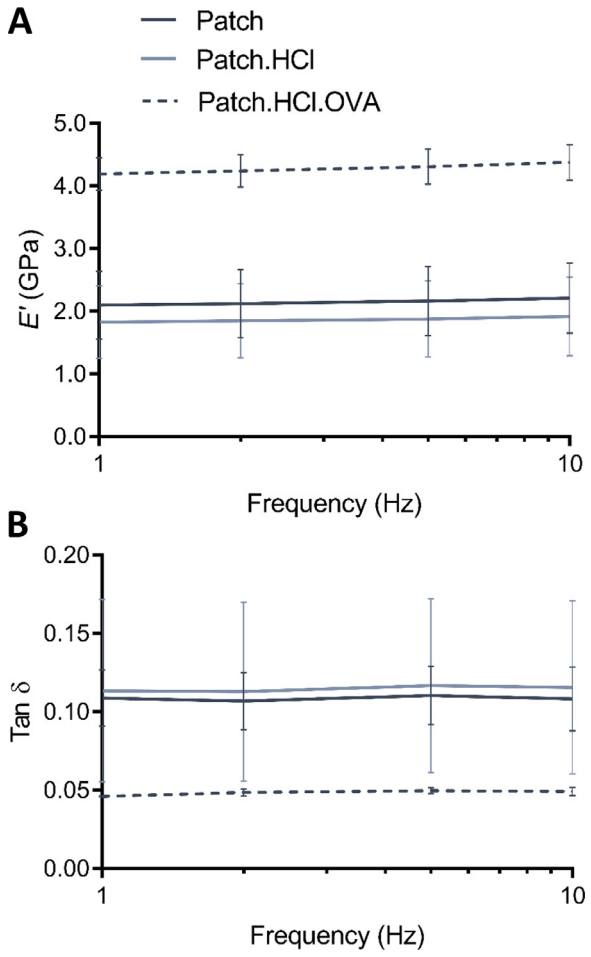

Fig. 5. Mechanical/viscoelastic properties of the patch before and after OVA loading using the tensile mode. (A) values obtained for *E'* and (B) tan *δ* displayed along a multi-frequency scan of 1, 2, 5 and 10 Hz at 25 °C in the dry state. Patch: $(CHI/HyA)_{100}$ membranes; Patch.HCl: HCl-treated $(CHI/HyA)_{100}$ membranes; Patch.HCl.OVA: OVA-loaded $(CHI/HyA)_{100}$ membranes using HCl treatment. Error bars are ± SD.

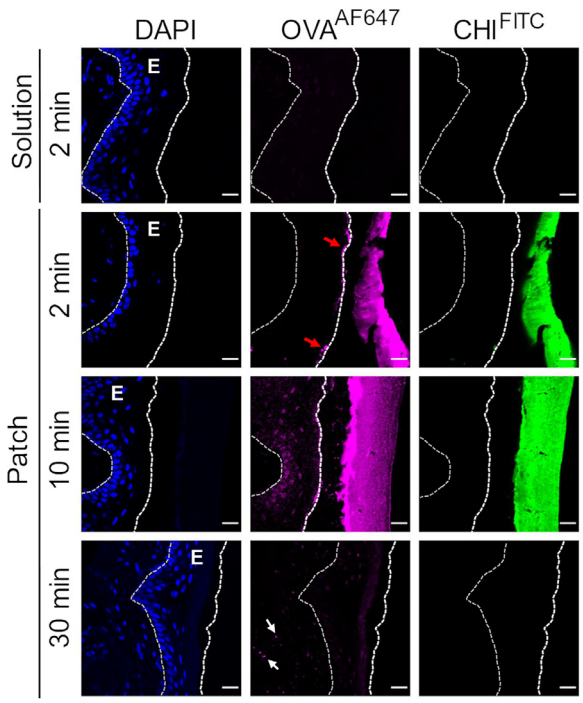

Fig. 7. Tissue penetration of OVA^{AF647} after patch administration. OVA^{F647} was administrated in liquid form or incorporated into a patch containing fluorescent CHI (CHI^{FITC}). Confocal microscopy pictures of mice tongue sections were taken after staining of cell nuclei with DAPI, 2 min after administration of OVA^{AF647} in solution or 2 min, 10 min and 30 min after administration of OVA^{AF647} incorporated into the patch $(CHI^{FITC}/HyA)_{100}$. Dotted lines correspond to the boundaries of the epithelium (E): grey lines (left) represent the basal lamina and white lines (right) the mucosa border. Arrows correspond to spots of OVA^{AF647}. Scale bar: 20 µm.

mucosal surface after administration by the patch. OVA^{AF647} entered the keratinized layer 10 min after patch administration and was observed in the epithelium among nucleated cells (red arrows, Fig. 7). The patch was not detectable 30 min after administration but OVA^{AF647} was slightly detectable deeply in the mucosa (white arrows, Fig. 7).

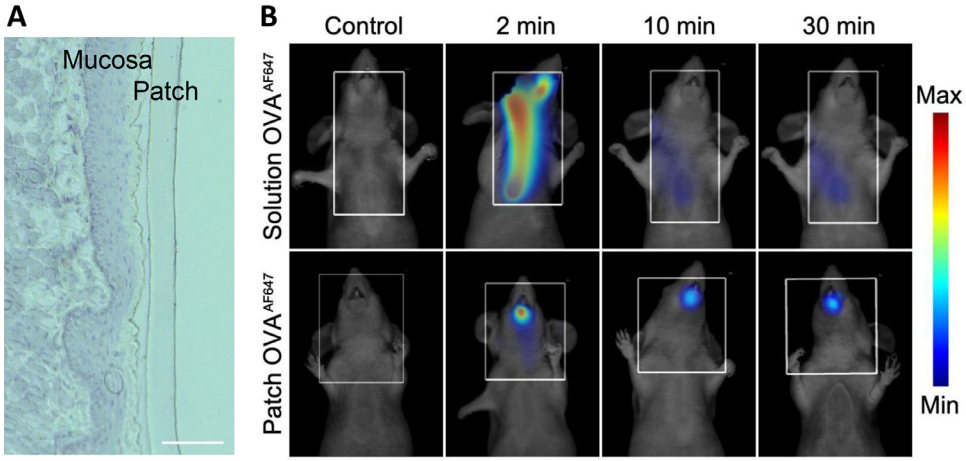

Fig. 6. Residence time of the patch on the sublingual mucosa. (**A**) Hematoxylin staining of the sublingual mucosa in contact with the patch $(CHI/HyA)_{100}$, 20 min after administration. Scale bar: 100 µm. (**B**) Fluorescence molecular tomography of OVA^{AF647} in solution or incorporated into the patch $(CHI/HyA)_{100}$. Fluorescent signal was detected 2, 10 or 30 min after administration.

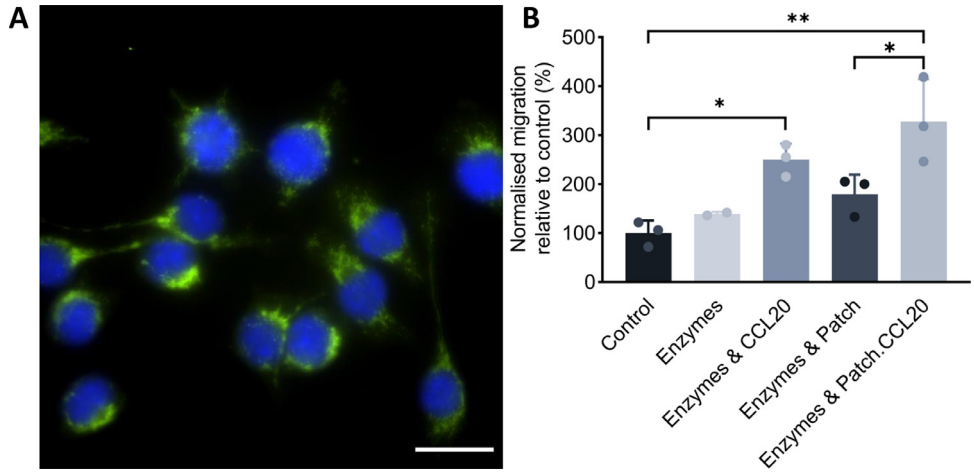

Fig. 8. Preservation of chemoattraction abilities of CCL20 cytokine incorporated into the patch. (**A**) Pictures of CCR6 labeling (green) in DC 2.4 cells stained with DAPI (blue) after 24h of CCL20 treatment. Scale bar: 20 µm. (**B**) *In vitro* chemotaxis ability of CCL20 released from the patch compared to CCL20 in the presence of salivary enzymes. A concentration of 25 ng/mL was used to evaluate migration of DC 2.4 cells. Growth medium, salivary enzymes alone and native membranes $(CHI/HyA)_{100}$ were used as negative controls. Each value provided is the average of triplicates of three independent experiments (N = 3). Statistical significance of differences between groups was determined using one-way ANOVA with Tukey's post hoc test; ns: non-significant, $^{*}p < 0.05$, $^{**}p < 0.01$. Error bars are ± SD. (For interpretation of the references to color in this figure legend, the reader is referred to the web version of this article.)

3.8. Bioactivity of the incorporated protein

To assess the functionality and bioactivity of a protein incorporated in the $(CHI/HyA)_{100}$ membrane, a chemoattractant cytokine (CCL20) was loaded into the assembly and collected after membrane degradation in artificial saliva. All conditions tested in this experiment were performed in the presence of artificial saliva to assess the bioactivity of the recombinant CCL20 in the present of salivary enzymes. The CCL20 cytokine was used as chemoattractant for murine DCs that possess the corresponding CCR6 receptor (Fig. 8A). The chemoattractant abilities of the cytokine were preserved inside the patch as a similar pattern of migration was found for CCL20 in solution and CCL20 collected after patch dissolution (Fig. 8B).

4. Discussion

Sublingual delivery of proteins is a promising alternative to *per oral* administration since it leads to an enhanced pharmacokinetic profile. This type of delivery also presents engaging results in allergy treatments as it can allow both local and systemic release of the antigens. Here a simple vectorization scaffold is presented based on the assembly of two polysaccharides: CHI and HyA. Both polyelectrolytes are combined by the LbL process. LbL assemblies may have two different growth behavior: linear or exponential growth; depending on several parameters such as molecular weight of polyelectrolytes or ionic strength [29,30]. Our results showed that thickness increased linearly with the number of layers (Fig. 1B), probably due to the high molecular weight of the polymers limiting their diffusion into the assembly.

Deposition of a hundred of bilayers of CHI and HyA with short deposition time permits to obtain a freestanding membrane with a thickness of around 12 µm (Fig. 1B and 1C). CHI was chosen as first and last layer for its mucoadhesive properties due to its positive charges interacting with negatively charged proteins of the mucus.

The choice of polysaccharides was motivated by the presence in the saliva of enzymes able to decompose these biomolecules by the degradation of glucosidic bonds (mainly α-amylase, hyaluronidase and lysozyme). Surprisingly, by shortening the time of the buildup process (short cycles: 3 min in polymer solution and 2 min of rinsing solution or long cycle: 6 min in polymer and 4 min in washing buffer) higher homogeneity in the thickness of the membranes was obtained (Fig. 1C). Those "short-cycles membranes" also present a faster degradation by artificial saliva during the first hour of contact with enzymes (Fig. 1F, insert). Interestingly, variation of the molecular weight of HyA (610 kDa or 1020 kDa) did not affect drastically the thickness of the membranes nor their kinetic of degradation (Fig. 1C and 1F). Being both large molecules, the difference in molecular weight did not affect the process of assembly of the membranes. Different types of polycations can be used in the membranes: CHI and VIS, a chitin-derived polysaccharide that presents a distinctive distribution of the N-acetylated groups. As it allows a slower degradation of the membrane (Figure S1B), CHI was purposefully chosen upon VIS in order to enhance the time of contact with the mucosa and lead to a slower release of the incorporated proteins. Additionally, the degradation time of the freestanding membranes could probably be increased by an additional crosslinking step [31].

Even though polymers, or the combination of polymers, can be considered as safe in terms of cell activity (Fig. 2), the systemic response of a tissue to a biomaterial can be visualized by an inflammatory response. Inflammation results in mucosa swelling due to liquid and immune cell infiltration. Mucosa thickness was therefore investigated as well as $MHC\text{-}II^{+}$ immune cells recruitment after membrane administration. As positive control, DNFB, an allergen known to promote inflammatory response in the oral cavity mucosa [28,32,33], was administered under the tongue of mice. Remarkably, the DNFB-induced mucosa swelling was concomitant with a decrease in the number of $MHC\text{-}II^{+}$ immune cells in the tissue 30 min after DNFB administration. This decrease could be due to the presence of an oedema (Fig. 3C) and the migration of antigen-presenting cells to lymphoid organs. The recruitment of circulating immune cells in the tissue can be observed by the increased number of $MHC\text{-}II^{+}$ cells 2h after DNFB administration (Figure S2B) as described after DNFB administration onto the inner faces of mice cheeks [33].

In the case of patch administration, neither the overall thickness of the mucosa nor the number of $MHC\text{-}II^{+}$ cells were affected (Fig. 3A, 3B and 3C). $MHC\text{-}II^{+}$ cells (DCs, B lymphocytes and macrophages) are sensor cells mostly residing within the mucosa. Together with epithelial cells, they are able to secrete pro-inflammatory cytokines to recruit resident or circulating immune cells locally. Six hours after patch administration, no persistence

of the inflammatory response was detected, as the profile of pro-inflammatory cytokines IL-1β, IL-6 and TNF-α was found to be similar as compared with PBS administration (Fig. 3D, 3E and 3F). These results highlighted the absence of inflammatory response due to the presence of the freestanding membrane whereas the DNFB show a persistence of pro-inflammatory cytokines.

The modulation or collapse of electrostatic interactions between the polyelectrolytes according to the pH also permitted the functionalization of the membranes by proteins. The native membranes loaded with protein were then called bioactive patches (Scheme 1).

The fluorescent model protein OVA^{AF647} was integrated in the membrane at pH 3 with an incorporation efficiency of around 98% that was maintained around 94% after 2h of rinsing with acetate buffer (pH 5.5) (Table 1 and Fig. 4A). Being the buffer used for membrane production, this solution would be an adapted candidate for the storage of the membranes in hydrated conditions. On the contrary, rinsing with PBS (pH 7.4) led to an incorporation of around 94%, and decreased to 69% after a 2 h-rinsing (Table 1 and Fig. 4A). The PBS-induced decrease in the entrapment efficiency is probably due to the high pH variation and ionic strength leading to the swelling of the membrane and subsequent disruption. This swelling could have avoided a full recovery of the initial physicochemical properties and subsequently led to protein leakage. The *in vitro* release of the protein when membrane is degraded by salivary enzymes after incorporation in HCl was 35% within 2 h (Fig. 4A) and more than 90% after 24 h (Table 1) highlighting the delivery efficiency of the system. As demonstrated in Fig. 4B and 4C, by adding a drop on the top of the membrane, the protein in HCl pH 3 was diffusing along the thickness of the assembly, forming a gradient with the highest concentration at the surface. By this effect, the patch became asymmetrical: with most of the protein at the surface, the directionality of the protein delivery towards the mucosa was controlled. Notably, the protein gradient allowed to avoid the addition of a backing layer protecting from protein leakage from the opposite side. In contrast, no gradient was observed by protein incorporation in NaCl (symmetric patch) (Figure S3B and S3C). The high incorporation rates of OVA^{AF647} in the patch either by incubation in HCl or NaCl open the possibility to incorporate a wide range of proteins that could be pH-sensitive and face denaturation at low pH.

Altogether, the release results provided a representation of the delivery profile mainly due to enzymatic degradation and pH variation. However, we can assume that, *in vivo*, some other mechanisms (for instance the mechanic forces due to mastication or swallowing) will intervene in the degradation process and therefore the release might be accelerated [34].

Protein incorporation modified the mechanical properties of the patch and led to an increase in stiffness (elastic modulus, *E'*) from 2 GPa to 4 GPa (Fig. 5A) that did not modify the handling properties of the patch. Previous work suggested that higher stiffness can result in a rapid burst release of the molecules loaded in films [35]. In addition, the values of around 0.1 for tan δ (Fig. 5B) reflected a viscoelastic performance, which is important for biomedical applications, since the living tissues and their biological constituents are also viscoelastic [36].

Once administered sublingually to mice, the membrane adapted its shape to the sublingual tissue (Fig. 6A) and was not visible by naked eye. The mucoadhesive properties of CHI were shown to be principally due to the electrostatic interaction between the positively charged amines on the polymer chains and the negative sialic acid residues on the mucin glycoprotein [37,38]. Besides, as the freestanding membrane was applied dry, suction forces induced by water uptake probably play a crucial role in mucoadhesion [16].

As illustrated in Fig. 6B, OVA^{AF647} delivered by the patch was detected as a concentrated signal in the mouth during at least 30 min, with mice let free to swallow and groom between the time points in order to closely mimic natural behavior. On the opposite, the liquid formulation was quickly washed-out in the saliva and disseminated through the digestive tract (signal already faint 10 min after administration of the liquid). These results highlighted the poor control of the administered liquid formulation and the requirement of animal contention to avoid swallowing. Indeed, the common procedure used for sublingual liquid administration includes a time of contention of the mice with heads maintained in anteflexion for 20 to 30 min to avoid swallowing [39–41]. Thus, by limiting animal manipulation, the use of a mucoadhesive patch improves animal wellbeing, simplifies the procedure of administration and would facilitate clinical translation.

As observed by confocal microscopy 2 min after administration, OVA^{AF647} signal at the mucosal surface is higher when delivered by the patch as compared to solution (Fig. 7), probably due to a local accumulation of the protein within the tissue and reduced wash-out of the protein in the saliva. The absence of signal of OVA^{AF647} delivered in liquid dosage may be explained by the administration protocol that did not include animal contention to avoid swallowing. Notably, 10 min after protein administration with a patch, OVA^{AF647} already penetrated into the sublingual epithelium that contains nucleated cells (red arrows, Fig. 7). The rapid penetration of OVA^{AF647} into the tissue can be explained by the permeation properties of CHI upon administration on the mucosa, as already described [9,22]. CHI could have permeabilized the tissue and facilitate passive protein penetration. These properties of the patch could thus avoid the use of chemical penetration enhancers such as sodium deoxycholate in the development of sublingual delivery platforms [11]. Therefore, it can be hypothesized that the co-delivery of the protein with patch fragments and especially CHI could improve protein penetration within the tissue, allowing a better delivery of the biomolecule. Moreover, this effect could be intensified with the enhanced retention time induced by the mucoadhesion of the membrane (Fig. 6). Indeed, even though the membrane does not appear on the images 30 min after administration (probably due to its degradation), the protein is present and is distributed deeply within the tissue (white arrows, Fig. 7). The decrease of protein fluorescence signal 30 min after administration could be explained by the clearance of the protein within the tissue and its uptake by immune cells such as APCs.

Besides efficient release, a protein delivery carrier has to present protective effect towards the cargo protein by maintaining its bioactivity. The use of a chemotactic cytokine (CCL20) incorporated into a $(CHI/HyA)_{100}$ membrane showed a preservation of the chemoattractant properties of the cytokine after release in the *in vitro* setting of enzymatic degradation (Fig. 8B). As a matter of fact, the use of polysaccharides that are components of the extra-cellular matrix would provide the biomaterial with the same properties, such as natural affinity of polysaccharides, and especially glycoaminoglycans, towards proteins [42]. Studies by circular dichroism measurements showed that the secondary structure of OVA in dry CHI film was partially preserved and that OVA was released under its native conformational form [43]. Additionally, the protective effect of polysaccharide based-LbL assemblies was also highlighted by Gilde *et al.* [44] where the preservation of the conformation of the growth factor BMP-2 was described by FTIR spectroscopy. Protective effect of protein bioactivity by LbL assemblies was attributed to the 'protein-friendly' environment provided by the high water content and porosity [45].

5. Conclusion

The development of a mucoadhesive patch made by LbL assembly of polysaccharides would open great promise as protein delivery carrier at mucosal sites. Here, we described that the loading of

$(CHI/HyA)_{100}$ freestanding membrane with the model protein OVA allowed an extended time of contact between the protein and the mucosa. As compared to a liquid formulation, the patch improved the amount of protein delivered through the mucosa. Besides, the administration of the patch being a simple procedure avoiding animal contention, its use could improve and facilitate the current protocols of sublingual administration.

Declaration of Competing Interest

The authors declare that they have no known competing financial interests or personal relationships that could have appeared to influence the work reported in this paper.

Acknowledgements

The authors would like to thank Thomas Barré from the AniCan plateform for his assistance and PHENOCAN for imaging devices [grant number ANR -11-EQPX-0035 PHENOCAN]; all the technical assistance provided at the Plateau de Biologie Expérimentale de la Souris, Lyon; Jérôme Sohier for assistance with DMA experiments; PLATIM for confocal microscopy; and Fabienne Jospin and Stéphane Paul for providing the Ho-1u-1 cells and technical assistance. This work was supported by the Agence Nationale de la Recherche contre le Sida et les Hépatites virales (ANRS) [grant number ECTZ60600]; the European Union's Horizon 2020 research and innovation programme [grant agreement number 751061]; Sidaction [grant number 11623] and the Agence Nationale de la Recherche (ANR) [grant number 192974].

Supplementary materials

Supplementary material associated with this article can be found, in the online version, at doi:10.1016/j.actbio.2021.04.024.

References

[1] Y. Sudhakar, K. Kuotsu, A.K. Bandyopadhyay, Buccal bioadhesive drug delivery - A promising option for orally less efficient drugs, J. Control. Release. 114 (2006) 15–40, doi:10.1016/j.jconrel.2006.04.012.
[2] T. Caon, L. Jin, C.M.O. Simões, R.S. Norton, J.A. Nicolazzo, Enhancing the buccal mucosal delivery of peptide and protein therapeutics, Pharm. Res. 32 (2015) 1–21, doi:10.1007/s11095-014-1485-1.
[3] A.K. Goyal, R. Singh, G. Chauhan, G. Rath, Non-invasive systemic drug delivery through mucosal routes, Artif. Cells, Nanomed. Biotechnol. 46 (2018) 539–551, doi:10.1080/21691401.2018.1463230.
[4] Z. Annabestani, S. Sharghi, S. Shahbazi, S.Mohseni Salehi Monfared, F. Karimi, E. Taheri, R. Heshmat, B. Larijani, Insulin Buccal Spray (Oral-Lyn) efficacy in Type 1 Diabetes, J. Diabetes Metab. Disord. 9 (18) (2010) http://jdmd.tums.ac.ir/index.php/jdmd/article/view/268. (accessed September 25, 2019).
[5] A.T. Jones, X. Shen, K.L. Walter, C.C. LaBranche, L.S. Wyatt, G.D. Tomaras, D.C. Montefiori, B. Moss, D.H. Barouch, J.D. Clements, P.A. Kozlowski, R. Varadarajan, R.R. Amara, HIV-1 vaccination by needle-free oral injection induces strong mucosal immunity and protects against SHIV challenge, Nat. Commun. (2019) 10, doi:10.1038/s41467-019-08739-4.
[6] P. Moingeon, V. Lombardi, V. Baron-Bodo, L. Mascarell, Enhancing allergen-presentation platforms for sublingual immunotherapy, J. Allergy Clin. Immunol. Pract. 5 (2017) 23–31, doi:10.1016/j.jaip.2016.07.020.
[7] H. Kraan, H. Vrieling, C. Czerkinsky, W. Jiskoot, G. Kersten, J.P. Amorij, Buccal and sublingual vaccine delivery, J. Control. Release. 190 (2014) 580–592, doi:10.1016/j.jconrel.2014.05.060.
[8] C. Thirion-Delalande, F. Gervais, C. Fisch, J. Cuiné, V. Baron-Bodo, P. Moingeon, L. Mascarell, Comparative analysis of the oral mucosae from rodents and non-rodents: Application to the nonclinical evaluation of sublingual immunotherapy products, PLoS One 12 (2017) 1–16, doi:10.1371/journal.pone.0183398.
[9] K. Klein, J.F.S. Mann, P. Rogers, R.J. Shattock, Polymeric penetration enhancers promote humoral immune responses to mucosal vaccines, J. Control. Release. 183 (2014) 43–50, doi:10.1016/j.jconrel.2014.03.018.
[10] M. Lal, J. White, C. Zhu, Preparing an adjuvanted thermoresponsive gel formulation for sublingual vaccination, Vaccine Adjuv. Methods Protoc. 1494 (2017) 153–163, doi:10.1007/978-1-4939-6445-1_11.
[11] J. Mašek, D. Lubasová, R. Lukáč, P. Turánek-Knotigová, P. Kulich, J. Plocková, E. Mašková, L. Procházka, Š. Koudelka, N. Sasithorn, J. Gombos, E. Bartheldyová, F. Hubatka, M. Raška, A.D. Miller, J. Turánek, Multi-layered nanofibrous mucoadhesive films for buccal and sublingual administration of drug-delivery and vaccination nanoparticles - important step towards effective mucosal vaccines, J. Control. Release. 249 (2017) 183–195, doi:10.1016/j.jconrel.2016.07.036.
[12] V.F. Patel, F. Liu, M.B. Brown, Advances in oral transmucosal drug delivery, J. Control. Release. (2011), doi:10.1016/j.jconrel.2011.01.027.
[13] S. Barua, H. Kim, K. Jo, C.W. Seo, T.J. Park, K. Bin Lee, G. Yun, K. Oh, J. Lee, Drug delivery techniques for buccal route: formulation strategies and recent advances in dosage form design, J. Pharm. Investig. 46 (2016) 593–613, doi:10.1007/s40005-016-0281-9.
[14] T. Vila, A.M. Rizk, A.S. Sultan, M.A. Jabra-Rizk, The power of saliva: antimicrobial and beyond, PLOS Pathog. 15 (2019) e1008058, doi:10.1371/journal.ppat.1008058.
[15] N. Salamat-Miller, M. Chittchang, T.P. Johnston, The use of mucoadhesive polymers in buccal drug delivery, Adv. Drug Deliv. Rev. (2005), doi:10.1016/j.addr.2005.07.003.
[16] J.D. Smart, Buccal drug delivery, Expert Opin. Drug Deliv. 2 (2005) 507–517, doi:10.1517/17425247.2.3.507.
[17] C. Colonna, I. Genta, P. Perugini, F. Pavanetto, T. Modena, M. Valli, C. Muzzarelli, B. Conti, 5-Methyl-pyrrolidinone chitosan films as carriers for buccal administration of proteins, AAPS Pharm. Sci. Tech. 7 (2006) 1–7, doi:10.1208/pt70370.
[18] F. Cui, C. He, M. He, C. Tang, L. Yin, F. Qian, C. Yin, Preparation and evaluation of chitosan-ethylenediaminetetraacetic acid hydrogel films for the mucoadhesive transbuccal delivery of insulin, J. Biomed. Mater. Res. - Part A. 89 (2009) 1063–1071, doi:10.1002/jbm.a.32071.
[19] N. Saint-Lu, S. Tourdot, A. Razafindratsita, L. Mascarell, N. Berjont, H. Chabre, A. Louise, L. Van Overtvelt, P. Moingeon, Targeting the allergen to oral dendritic cells with mucoadhesive chitosan particles enhances tolerance induction, Allergy Eur. J. Allergy Clin. Immunol. 64 (2009) 1003–1013, doi:10.1111/j.1398-9995.2009.01945.x.
[20] I. Ayensu, J.C. Mitchell, J.S. Boateng, Development and physico-mechanical characterisation of lyophilised chitosan wafers as potential protein drug delivery systems via the buccal mucosa, Colloids Surf. B Biointerfaces 91 (2012) 258–265, doi:10.1016/j.colsurfb.2011.11.004.
[21] M.C. Bonferoni, G. Sandri, S. Rossi, F. Ferrari, C. Caramella, Chitosan and its salts for mucosal and transmucosal delivery, Expert Opin. Drug Deliv. 6 (2009) 923–939, doi:10.1517/17425240903114142.
[22] A. Kumar, A. Vimal, A. Kumar, Why Chitosan? From properties to perspective of mucosal drug delivery, Int. J. Biol. Macromol. 91 (2016) 615–622, doi:10.1016/j.ijbiomac.2016.05.054.
[23] G. Decher, Fuzzy nanoassemblies: toward layered polymeric multicomposites, Science 277 (80) (1997) 1232–1237, doi:10.1126/science.277.5330.1232.
[24] S.G. Caridade, C. Monge, J. Almodóvar, R. Guillot, J. Lavaud, V. Josserand, J.L. Coll, J.F. Mano, C. Picart, Myoconductive and osteoinductive free-standing polysaccharide membranes, Acta Biomater. 15 (2015) 139–149, doi:10.1016/j.actbio.2014.12.027.
[25] M. Bertolini, T. Sobue, A. Thompson, A. Dongari-Bagtzoglou, Chemotherapy induces oral mucositis in mice without additional noxious stimuli, Transl. Oncol. 10 (2017) 612–620, doi:10.1016/j.tranon.2017.05.001.
[26] J. Pytko-Polonczyk, A. Jakubik, A. Przeklasa-Bierowiec, B. Muszynska, Artificial saliva and its use in biological experiments, J. Physiol. Pharmacol. 68 (2017) 807–813.
[27] M.A. Pogrel, M.A. Low, R. Stern, Hyaluronan and its regulation in human saliva by hyaluronidase and its inhibitors, 45 (2003) 85–91.
[28] M.Le Borgne, N. Etchart, A. Goubier, S.A. Lira, J.C. Sirard, N. Van Rooijen, C. Caux, S. Aït-Yahia, A. Vicari, D. Kaiserlian, B. Dubois, Dendritic cells rapidly recruited into epithelial tissues via CCR6/CCL20 are responsible for CD8 + T cell crosspriming in vivo, Immunity 24 (2006) 191–201, doi:10.1016/j.immuni.2006.01.005.
[29] C. Picart, J. Mutterer, L. Richert, Y. Luo, G.D. Prestwich, P. Schaaf, J.C. Voegel, P. Lavalle, Molecular basis for the explanation of the exponential growth of polyelectrolyte multilayers, Proc. Natl. Acad. Sci. U. S. A. 99 (2002) 12531–12535, doi:10.1073/pnas.202486099.
[30] J. Borges, J.F. Mano, Molecular interactions driving the layer-by-layer assembly of multilayers, Chem. Rev. 114 (2014) 8883–8942, doi:10.1021/cr400531v.
[31] M.J. Cardoso, S.G. Caridade, R.R. Costa, J.F. Mano, Enzymatic degradation of polysaccharide-based layer-by-layer structures, Biomacromolecules 17 (2016) 1347–1357, doi:10.1021/acs.biomac.5b01742.
[32] W. Hirunwidchayarat, E. Furusawa, S. Kang, T. Ohno, S. Takeuchi, S. Rungsiyanont, M. Azuma, Site-specific regulation of oral mucosa-recruiting CD8+T cells in a mouse contact allergy model, Biochem. Biophys. Res. Commun. 490 (2017) 1294–1300, doi:10.1016/j.bbrc.2017.07.012.
[33] I. Effendy, H. Löffler, H.I. Maibach, Epidermal cytokines in murine cutaneous irritant responses, J. Appl. Toxicol. 20 (2000) 335–341 L, doi:10.1002/1099-1263(200007/08)20:4⟨335::AID-JAT698⟩3.0.CO;2.
[34] O. Etienne, A. Schneider, C. Taddei, L. Richert, P. Schaaf, J.C. Voegel, C. Egles, C. Picart, Degradability of polysaccharides multilayer films in the oral environment: an in vitro and in vivo study, Biomacromolecules 6 (2005) 726–733, doi:10.1021/bm049425u.
[35] P.M. Castro, P. Fonte, A. Oliveira, A.R. Madureira, B. Sarmento, M.E. Pintado, Optimization of two biopolymer-based oral films for the delivery of bioactive molecules, Mater. Sci. Eng. C. 76 (2017) 171–180, doi:10.1016/j.msec.2017.02.173.
[36] J.F. Mano, R.L. Reis, A.M. Cunha, Dynamic mechanical analysis in polymers for medical applications, in: R.L. Reis, D. Cohn (Eds.), Polym. Based Syst. Tissue Eng. Replace. Regen., NATO Scien, Springer, Dordrecht, 2002, pp. 139–164, doi:10.1007/978-94-010-0305-6_10.
[37] R.J. Soane, M. Frier, A.C. Perkins, N.S. Jones, S.S. Davis, L. Illum, Evaluation of

the clearance characteristics of bioadhesive systems in humans, Int. J. Pharm. 178 (1999) 55–65, doi:10.1016/S0378-5173(98)00367-6.
[38] I.A. Sogias, A.C. Williams, V.V. Khutoryanskiy, Why is chitosan mucoadhesive? Biomacromolecules 9 (2008) 1837–1842, doi:10.1021/bm800276d.
[39] G.K. Pedersen, T. Ebensen, I.H. Gjeraker, S. Svindland, G. Bredholt, C.A. Guzmán, R.J. Cox, Evaluation of the sublingual route for administration of influenza H5N1 virosomes in combination with the bacterial second messenger c-di-GMP, PLoS One 6 (2011), doi:10.1371/journal.pone.0026973.
[40] S. Gallorini, M. Taccone, A. Bonci, F. Nardelli, D. Casini, A. Bonificio, S. Kommareddy, S. Bertholet, D.T. O'Hagan, B.C. Baudner, Sublingual immunization with a subunit influenza vaccine elicits comparable systemic immune response as intramuscular immunization, but also induces local IgA and TH17 responses, Vaccine 32 (2014) 2382–2388, doi:10.1016/j.vaccine.2013.12.043.
[41] C. Hervouet, C. Luci, N. Çuburu, M. Cremel, S. Bekri, L. Vimeux, C. Marañon, C. Czerkinsky, A. Hosmalin, F. Anjuère, Sublingual immunization with an HIV subunit vaccine induces antibodies and cytotoxic T cells in the mouse female genital tract, Vaccine 28 (2010) 5582–5590, doi:10.1016/j.vaccine.2010.06.033.
[42] C. Laguri, F. Arenzana-Seisdedos, H. Lortat-Jacob, Relationships between glycosaminoglycan and receptor binding sites in chemokines-the CXCL12 example, Carbohydr. Res. 343 (2008) 2018–2023, doi:10.1016/j.carres.2008.01.047.
[43] J. Becerra, G. Sudre, I. Royaud, R. Montserret, B. Verrier, C. Rochas, T. Delair, L. David, Tuning the hydrophilic/hydrophobic balance to control the structure of chitosan films and their protein release behavior, AAPS Pharm. Sci. Tech. 18 (2017) 1070–1083, doi:10.1208/s12249-016-0678-9.
[44] F. Gilde, O. Maniti, R. Guillot, J.F. Mano, D. Logeart-Avramoglou, F. Sailhan, C. Picart, Secondary structure of rhBMP-2 in a protective biopolymeric carrier material, Biomacromolecules 13 (2012) 3620–3626, doi:10.1021/bm3010808.
[45] R. Guillot, F. Gilde, P. Becquart, F. Sailhan, A. Lapeyrere, D. Logeart-Avramoglou, C. Picart, The stability of BMP loaded polyelectrolyte multilayer coatings on titanium, Biomaterials 34 (2013) 5737–5746, doi:10.1016/j.biomaterials.2013.03.067.